Study of Magnetohydrodynamic Surface Waves on Liquid Gallium

by

Hantao Ji, William Fox, David Pace, and H.L. Rappaport

May 2004

**PRINCETON PLASMA PHYSICS LABORATORY
PRINCETON UNIVERSITY, PRINCETON, NEW JERSEY**

PPPL Reports Disclaimer

This report was prepared as an account of work sponsored by an agency of the United States Government. Neither the United States Government nor any agency thereof, nor any of their employees, makes any warranty, express or implied, or assumes any legal liability or responsibility for the accuracy, completeness, or usefulness of any information, apparatus, product, or process disclosed, or represents that its use would not infringe privately owned rights. Reference herein to any specific commercial product, process, or service by trade name, trademark, manufacturer, or otherwise, does not necessarily constitute or imply its endorsement, recommendation, or favoring by the United States Government or any agency thereof. The views and opinions of authors expressed herein do not necessarily state or reflect those of the United States Government or any agency thereof.

Availability

This report is posted on the U.S. Department of Energy's Princeton Plasma Physics Laboratory Publications and Reports web site in Fiscal Year 2004. The home page for PPPL Reports and Publications is: http://www.pppl.gov/pub_report/

DOE and DOE Contractors can obtain copies of this report from:

U.S. Department of Energy
Office of Scientific and Technical Information
DOE Technical Information Services (DTIS)
P.O. Box 62
Oak Ridge, TN 37831

Telephone: (865) 576-8401

Fax: (865) 576-5728

Email: reports@adonis.osti.gov

This report is available to the general public from:

National Technical Information Service
U.S. Department of Commerce
5285 Port Royal Road
Springfield, VA 22161

Telephone: 1-800-553-6847 or
(703) 605-6000

Fax: (703) 321-8547

Internet: http://www.ntis.gov/ordering.htm

Study of Magnetohydrodynamic Surface Waves on Liquid Gallium

Hantao Ji,[*] William Fox,[†] and David Pace[‡]

Plasma Physics Laboratory, Princeton University, Princeton, New Jersey

H.L. Rappaport

Institute for Fusion Studies, University of Texas at Austin, Austin, Texas

(Dated: May 11, 2004)

Abstract

Magnetohydrodynamic (MHD) surface waves on liquid gallium are studied theoretically and experimentally in the small magnetic Reynolds number limit. A linear dispersion relation is derived when a horizontal magnetic field and a horizontal electric current is imposed. No wave damping is found in the shallow liquid limit while waves always damp in the deep liquid limit with a magnetic field parallel to the propagation direction. When the magnetic field is weak, waves are weakly damped and the real part of the dispersion is unaffected, while in the opposite limit waves are strongly damped with shortened wavelengths. In a table-top experiment, planar MHD surface waves on liquid gallium are studied in detail in the regime of weak magnetic field and deep liquid. A non-invasive diagnostic accurately measures surface waves at multiple locations by reflecting an array of lasers off the surface onto a screen, which is recorded by an Intensified-CCD camera. The measured dispersion relation is consistent with the linear theory with a reduced surface tension likely due to surface oxidation. In excellent agreement with linear theory, it is observed that surface waves are damped only when a horizontal magnetic field is imposed parallel to the propagation direction. No damping is observed under a perpendicular magnetic field. The existence of strong wave damping even without magnetic field suggests the importance of the surface oxide layer. Implications to the liquid metal wall concept in fusion reactors, especially on the wave damping and a Rayleigh-Taylor instability when the Lorentz force is used to support liquid metal layer against gravity, are discussed.

PACS numbers:

I. INTRODUCTION

The effect of a magnetic field and electric current on the dynamics of liquid metals with a free surface facing a vacuum or a non-conducting fluid (*e.g.* air), is a century-old problem, studied first by Northrup[1]. However, the progress in their understanding has been very limited, especially in the laboratory. Recently, a new interest has arisen in this problem: electrically conducting liquids, such as liquid lithium or liquid salt (Flibe), are proposed as the material facing the burning plasma in fusion reactors, directly handling the heat flux and breeding tritium from neutrons[2–5]. The liquid is typically under extreme mechanical and thermal stresses due to the required fast flows and the high heat flux on the free surface[2]. In addition, a typical magnetic fusion reactor uses a strong magnetic field (on the order of 10 Tesla) to confine plasma. Often, an electric current is driven in the conducting, plasma-facing material by either induction or an externally supplied voltage. The existence of a magnetic field and current adds complexity to the already turbulent nature of such free-surface flows. In addition, unstable plasma modes can be coupled to free-surface modes of liquid wall[6]. A comprehensive understanding of dynamics of such liquids in magnetic fields and with applied currents becomes crucial for the success of this new application.

A first step towards this goal is to understand the physics of magnetohydrodynamic (MHD) surface waves in a static pool subject to an externally applied magnetic field and a current parallel to the unperturbed surface. The past work on the subject, including theory and experiment, has been very limited. Murty[7] studied linear waves when the externally applied magnetic field and current are in the same direction. An instability due to the pinch force (the Lorentz force directed inward to the fluid) was found, consistent with the phenomena described by Northrup[1] when only the current was imposed. Similar instabilities in a current-carrying cylinder along an axial magnetic field were also studied[8,9].

The first serious theoretical effort on a more general case, where the magnetic field has an arbitrary angle with current was made by Shercliff[10]. When the resultant Lorentz force is upward and is larger than gravity, the surface becomes unstable, as in the Rayleigh-Taylor instability. Earlier experiments had observed this instability[11,12]. Shercliff also found that a magnetic field and current introduces anisotropy in the propagation of surface waves. In addition, Sherclif estimated the effects of ohmic damping when the waves propagate parallel to the magnetic field. A similar theoretical study[13] was performed earlier on the subject but

using more involved calculations. In both these studies, the magnetic field generated by the current was ignored so that the pinch instability was absent in the analysis.

Another assumption used by Sharcliff was that the fluid velocity is two-dimensional, restricted to the plane spanned by the vertical (gravity) and the vector of wave propagation. This assumption was relaxed only more than 20 years later by Shishkov[14] and Korovin[15]. While the former author did not elaborate on the consequences, the latter author claimed that the resultant dispersion relation and damping rate are significantly different except for some special cases.

Experimentally, there have been almost no quantitative studies of wave propagation and damping when a magnetic field or current is imposed parallel to the free surface. Experiments that we referred to earlier[1,11,12] focused on the pure growing mode due to the pinch force. The only published experiment found[16] used a magnetic field oscillating in time to simulate a perfectly conducting liquid metal facing to DC field.

Herein we report a detailed theoretical and experimental study of the propagation and damping of MHD surface waves on liquid gallium. We begin in Sec.II with a detailed derivation of the linear dispersion relation when both magnetic field and current are parallel to the free surface. It is found that the 2-D assumption made by Sharcliff[10] does not impact the result, in contrast to the claims of Korovin[15]. In Sec.III and IV, we describe the experimental apparatus and results in detail. The dispersion relation and damping rates are measured and compared to the linear theory. Implications to the application of a liquid metal first wall in fusion reactors are discussed in Sec.V, followed by conclusions in Sec.VI.

II. LINEAR THEORY OF MHD SURFACE WAVES

A. Basic assumptions and governing equations

A flat layer of liquid metal with a free surface is assumed to be at rest sitting on top of a non-conducting wall with large horizontal dimensions compared to the layer thickness, h. We define a Cartesian coordinate system as shown in Fig.(1), where surface waves are assumed to propagate along the x direction with a wavevector $\boldsymbol{k} = (k, 0, 0)$. Following Sharcliff[10], the externally imposed magnetic field and electric current are homogeneous and parallel to the free surface at rest: $\boldsymbol{B}_0 = (B_{0x}, B_{0y}, 0)$ and $\boldsymbol{j}_0 = (j_{0x}, j_{0y}, 0)$. Here, the subscripts 0 and 1

denote equilibrium values and oscillatory values in the wave, respectively.

An internal pressure profile, $p_0(z)$, is set up to maintain static equilibrium ($\boldsymbol{V}_0 = 0$) by

$$\frac{\partial p_0}{\partial z} = -\rho g + j_{0x}B_{0y} - j_{0y}B_{0x}, \tag{1}$$

where ρ is the mass density of liquid metal and $g = 9.8$ m/s^2 is the gravitational acceleration. Here, the magnetic field generated by the current flowing internally in the liquid metal, B_{self}, which is on the order of $\mu_0 j_0 h$ is assumed to be negligible compared to the imposed B_0. (μ_0 is magnetic permeability of the vacuum and, by assumption, the liquid metal.) Ignoring the self-B field enforces the equilibrium Lorentz force, $\boldsymbol{j}_0 \times \boldsymbol{B}_0$, to be directed only vertically in the z direction, eliminating the pinch instability[7] discussed earlier. We note that this assumption is valid in the applications for fusion reactors, where the external magnetic field is typically strong and the needed external current, if any, is small. Assuming $j_0 \sim \rho g/B_0$, an estimate is given by $B_{\text{self}}/B_0 \simeq \mu_0 j_0 h/B_0 \simeq \mu_0 \rho g h/B_0^2 \simeq 3 \times 10^{-7}$ for the typical conditions[2] of $\rho = 500$ kg/m^3 (lithium), $h = 5$ mm, and $B_0 = 10$ Tesla. This assumption is also well satisfied in the experiments reported later in this paper where no external current is imposed.

An important parameter characterizing dynamics of the liquid metal layer is the magnetic Reynolds number, $R_{\text{m}} = \mu_0 V h/\eta$ where V is a characteristic velocity and η is the electrical resistivity. For the present problem on surface waves in a static liquid metal layer, an appropriate choice for V is the phase velocity $V_{\text{ph}} = \omega/k$, where ω is the angular frequency. For typical parameters available in the experiments described later, $R_{\text{m}} \sim 10^{-2} \ll 1$. In this small R_{m} limit, the wave-induced magnetic field is negligible, resulting in the so-called electrostatic approximation to Faraday's law, $\partial \boldsymbol{B}_1/\partial t = -\boldsymbol{\nabla} \times \boldsymbol{E}_1 \approx 0$, so the perturbing
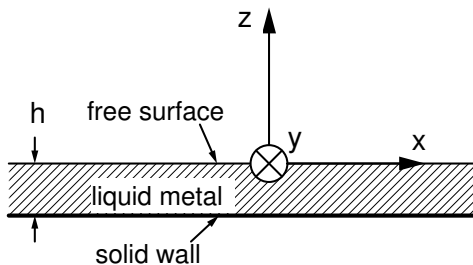

FIG. 1: The coordinate for surface wave analysis. The waves are assumed to propagate along x direction while the magnetic field and current are homogeneous and parallel to the free surface: $\boldsymbol{B}_0 = (B_{0x}, B_{0y}, 0)$ and $\mathbf{j}_0 = (j_{0x}, j_{0y}, 0)$.

electric field must take the form $\boldsymbol{E}_1 = -\boldsymbol{\nabla}\phi$, while Ampere's law simply reduces to $\boldsymbol{\nabla}\cdot\boldsymbol{j}_1 = 0$. In addition, the corresponding wave-Lorentz force is negligible, *i.e.*, $\boldsymbol{j}_1 \times \boldsymbol{B}_0 \gg \boldsymbol{j}_0 \times \boldsymbol{B}_1$. As a result, linear waves in the liquid metal layer at rest ($\boldsymbol{V}_0 = 0$) are well described by a set of incompressible, inviscid but resistive MHD equations,

$$\rho\frac{\partial \boldsymbol{V}_1}{\partial t} = \boldsymbol{j}_1 \times \boldsymbol{B}_0 - \boldsymbol{\nabla}p_1 \tag{2}$$

$$-\boldsymbol{\nabla}\phi + \boldsymbol{V}_1 \times \boldsymbol{B}_0 = \eta\boldsymbol{j}_1 \tag{3}$$

$$\boldsymbol{\nabla} \cdot \boldsymbol{j}_1 = 0 \tag{4}$$

$$\boldsymbol{\nabla} \cdot \boldsymbol{V}_1 = 0 \tag{5}$$

where $\boldsymbol{V}_1$ and p_1 are the perturbed velocity field and pressure, respectively. In the momentum equation, the linearizing condition to ignore the convective derivative terms $\rho(\boldsymbol{V}_1 \cdot \boldsymbol{\nabla})\boldsymbol{V}_1$ can be shown to be $ka \ll 1$, where a is the amplitude of the surface displacement. ka is the wave "steepness." The linear theory is thus valid when the waves are not steep; effects like breaking waves are inherently non-linear phenomena where the steepness becomes infinite. Finally, note that every oscillatory quantity, $f(t, x, z)$, can be assumed to take the form of $f(z)\exp[i(\omega t - kx)]$, where $f(z)$ is a function of only z. The boundary conditions shall be discussed in the next section.

B.   Solving velocity and current fields

To satisfy the incompressibility condition, Eq.(5), the velocity field can be assumed to take the following shape

$$\boldsymbol{V}_1(x, z) = \boldsymbol{y} \times \boldsymbol{\nabla}\psi(x, z) + V_{1y}(x, z)\boldsymbol{y}, \tag{6}$$

so that $V_{1x} = \partial\psi/\partial z$ and $V_{1z} = -\partial\psi/\partial x$. (Unlike Shercliff[10], we include V_{1y} for the sake of completeness.) Using Eq.(6), Ohm's law, Eq.(3) or

$$\eta\boldsymbol{j}_1 = -\boldsymbol{\nabla}(\phi - B_{0y}\psi) + V_{1z}B_{0x}\boldsymbol{y} - V_{1y}B_{0x}\boldsymbol{z}, \tag{7}$$

must satisfy Eq.(4) to yield

$$\eta\boldsymbol{\nabla} \cdot \boldsymbol{j}_1 = -\nabla^2(\phi - B_{0y}\psi) - \frac{\partial V_{1y}}{\partial z}B_{0x} = 0. \tag{8}$$

5

Since $\partial p_1/\partial y = 0$, the y component of Eq.(2) simply becomes $\rho\partial V_{1y}/\partial t = (\boldsymbol{j}_1 \times \boldsymbol{B}_0)_y = j_{1z}B_{0x}$, where j_{1z} is supplied by Eq.(7). Solving for V_{1y} yields

$$V_{1y} = -\frac{\partial(\phi - B_{0y}\psi)}{\partial z}\frac{B_{0x}}{i\rho\eta\omega + B_{0x}^2}. \tag{9}$$

Hence Eq.(8) is rewritten to a simple form of

$$\frac{\partial^2 \Phi}{\partial z^2} = K^2 \Phi$$

where $\Phi \equiv \phi - B_{0y}\psi$ and $K^2 \equiv k^2(1 - iB_{0x}^2/\rho\eta\omega) \equiv k^2(1 - i\alpha)$. Solving the above equation using the insulating boundary condition ($j_{1z}|_{z=-h} = 0$) or equivalently $j_{1z}|_{z=-h} \propto V_{1y}|_{z=-h} \propto \partial\Phi/\partial z|_{z=-h} = 0$, yields the solutions for Φ

$$\Phi \equiv \phi - B_{0y}\psi = C\cosh[K(z+h)]\exp[i(\omega t - kx)] \tag{10}$$

where C is a constant.

A second equation is obtained through the y component of the curl of Eq.(2), $\rho\partial(\boldsymbol{\nabla} \times \boldsymbol{V}_1)_y/\partial t = [\boldsymbol{\nabla} \times (\boldsymbol{j}_1 \times \boldsymbol{B}_0)]_y$, which reduces to

$$\rho\frac{\partial\nabla^2\psi}{\partial t} = B_{0x}\frac{\partial j_{1y}}{\partial x} = \frac{B_{0x}^2}{\eta}\frac{\partial V_{1z}}{\partial x} = -\frac{B_{0x}^2}{\eta}\frac{\partial^2\psi}{\partial x^2}$$

by using Eq.(7). Therefore, we again have

$$\frac{\partial^2\psi}{\partial z^2} = K^2\psi,$$

which can be solved by using the boundary condition $V_{1z}|_{z=-h} = -\partial\psi/\partial x|_{z=-h} = 0$ to yield

$$\psi = A\sinh[K(z+h)]\exp[i(\omega t - kx)] \tag{11}$$

where A is a constant. With solutions for Φ and ψ given by Eqs.(10,11), the velocity and current fields are known through Eqs.(6,7,9), except the constants A and C:

$$\boldsymbol{V}_1 = \frac{\partial\psi}{\partial z}\boldsymbol{x} - \frac{1}{B_{0x}}\frac{\partial\Phi}{\partial z}\left(1 - \frac{1}{1 - i\alpha}\right)\boldsymbol{y} - \frac{\partial\psi}{\partial x}\boldsymbol{z} \tag{12}$$

$$\eta\boldsymbol{j}_1 = -\frac{\partial\Phi}{\partial x}\boldsymbol{x} - B_{0x}\frac{\partial\psi}{\partial x}\boldsymbol{y} - \frac{\partial\Phi}{\partial z}\frac{1}{1 - i\alpha}\boldsymbol{z}. \tag{13}$$

6

C.   Free-surface boundary conditions

Let $z = \delta(t, x) = \delta \exp(i(\omega t - kx))$ represent the wavy free surface of the liquid metal. By definition,

$$\frac{\partial \delta}{\partial t} = V_{1z}|_{z=\delta} \approx V_{1z}|_{z=0} = -\left.\frac{\partial \psi}{\partial x}\right|_{z=0}$$

where "$\approx$"represents linear approximation, again satisfied for small wave steepness. Thus

$$\delta = A\frac{k}{\omega}\sinh(Kh)\exp[i(\omega t - kx)]. \tag{14}$$

The second boundary condition on the free-surface is that the current must be confined within the liquid metal, *i.e.*,

$$(\boldsymbol{j}_0 + \boldsymbol{j}_1|_{z=0}) \cdot \hat{\boldsymbol{n}} = 0, \tag{15}$$

where $\hat{\boldsymbol{n}}$ is the unit normal vector of the free surface. Let $f = z - \delta$, then we have

$$\hat{\boldsymbol{n}} = \boldsymbol{\nabla}f/|\boldsymbol{\nabla}f| = iA\frac{k^2}{\omega}\sinh(Kh)\exp[i(\omega t - kx)]\boldsymbol{x} + \boldsymbol{z}.$$

Taking the first order of Eq.(15), we have $j_{0x}n_x + j_{1z} = 0$ which becomes $C = iAj_{0x}K\eta/\omega$, leading to

$$\Phi = iA\frac{j_{0x}K\eta}{\omega}\cosh[K(z+h)]\exp[i(\omega t - kx)]. \tag{16}$$

D.   Dispersion relation

Without losing generality, let the ambient pressure above the liquid metal be zero, which must balance with the pressure right underneath the surface plus a force due to surface tension,

$$p_1|_{z=0} + \left.\frac{\partial p_0}{\partial z}\right|_{z=0}\delta + T\frac{\partial^2 \delta}{\partial x^2} = 0,$$

where T is the surface tension coefficient. Thus, using Eq.(1), we have

$$p_1|_{z=0} = A\frac{k}{\omega}\sinh(Kh)(\rho g - j_{0x}B_{0y} + j_{0y}B_{0x} + k^2 T)\exp[i(\omega t - kx)].$$

Applying this to the x component of Eq.(2),

$$\rho\frac{\partial V_{1x}}{\partial t} = -\frac{\partial p_1}{\partial x} - j_{1z}B_{0y}, \tag{17}$$

at $z = 0$ yields the dispersion relation for MHD surface waves

$$\rho\omega^2 = (\rho g + j_{0y}B_{0x} + k^2 T)\frac{k^2}{K}\tanh(Kh), \tag{18}$$

where $K^2 = k^2(1 - i\alpha)$ and $\alpha = B_{0x}^2/\rho\eta\omega$.

A few observations on the above dispersion relation, Eq.(18), are in order. First, setting $\boldsymbol{B}_0 = \boldsymbol{j}_0 = 0$ recovers the usual surface wave dispersion relation in neutral fluid,

$$\rho\omega^2 = (\rho g + k^2 T)k\tanh(kh).$$

Second, the added imaginary component, α, due to the magnetic field along the propagation direction, will cause the surface wave to damp due to ohmic heating. A transverse magnetic field has no effect at all on the waves, because the perturbing motion does not bend field lines. The wave damping shall be discussed in detail in the later sections. Third, the second component of Lorentz force in the vertical direction, $j_{0x}B_{0y}$, does not appear in the dispersion relation. The reason for the disappearance can be found in Eq.(17) where the second term on the right hand side, $-j_{1z}B_{0y}$, cancels the $j_{0x}B_{0y}$ term contained in the first term, $-\partial p_1/\partial x$. Since the perturbed current, j_{1z}, arises because of the waviness of the free surface when a uniform current, j_{0x}, flows along the propagation (x) direction, this is a special effect due to the free surface facing a non-conducting fluid or vacuum. However, this effect leads to an instability (Rayleigh-Taylor instability) when the Lorentz force is used to put a liquid metal layer up against gravity in applications like in fusion reactor[2]. The detailed implications shall be discussed in Sec.V.

E. Shallow and deep liquid limits

It is useful to take some limits for the obtained dispersion relation. The shallow liquid limit, defined as $kh \ll 1$, simplifies the dispersion relation by using $\tanh(Kh) \approx Kh$ to

$$\rho\omega^2 = (\rho g + j_{0y}B_{0x} + k^2 T)k^2 h,$$

The damping effect does not appear to first order in kh. Intuitively, the waves damp by ohmic dissipation of energy put into bending magnetic field lines. But, in the shallow limit, fluid motion in the vertical direction is suppressed, so waves do not store energy in bending field lines, and hence are not damped.

The opposite limit, or the deep liquid limit, $kh \gg 1$ and thus $\tanh(Kh) \approx 1$, leads to the dispersion relation,

$$\rho\omega^2 = (\rho g + j_{0y}B_{0x} + k^2 T)\frac{k}{\sqrt{1 - i\alpha}}. \tag{19}$$

8

When B_{0x} is weak so that $\alpha \ll 1$ and $(1 - i\alpha)^{-1/2} \approx 1 + i\alpha/2$, and if we assume that ω is real and k is complex, $k = k_r + i k_i$ ($k_r \gg k_i$), the real and imaginary parts of Eq.(19) give

$$\rho\omega^2 = (\rho g + j_{0y} B_{0x} + k_r^2 T) k_r \tag{20}$$

$$k_i = -\frac{B_{0x}^2 \omega k_r}{2\eta(\rho\omega^2 + 2T k_r^3)}, \tag{21}$$

respectively. The convective damping rate is given by Eq.(21), which reduces to simple $k_i = -(\alpha/2)k_r$ if $T = 0$. A small shortening of the wavelength enters in second order in α.

Here it is appropriate to provide a heuristic derivation of the damping rate Eq.(21). The ohmic dissipation is estimated as

$$\eta j^2 \simeq \eta \left(\frac{vB}{\eta}\right)^2 = \frac{v^2 B^2}{\eta},$$

where v is the characteristic fluid velocity. Then the wave energy decays as

$$\frac{\partial}{\partial t}\left(\frac{1}{2}\rho v^2\right) = -\frac{B^2}{\eta}v^2,$$

which leads to

$$a(t) = a_0 \exp\left[-\frac{B^2}{\rho\eta}t\right]$$

since $v = \partial a/\partial t = \omega a$. Setting $t = x/v_{\rm ph} = kx/\omega$ in the above equation leads to $a(x) = a_0 \exp(-k_i x)$, where

$$k_i = -\frac{B^2 k}{\rho\eta\omega}.$$

This is consistent with Eq.(21) within a factor of 2 when the surface tension is ignored.

When B_{0x} is strong so that $\alpha \gg 1$, the dispersion relation relaxes to a different form,

$$\rho\omega^2 = (\rho g + j_{0y} B_{0x} + k^2 T)\frac{k}{\sqrt{2\alpha}}(1 + i). \tag{22}$$

If ω is set to be real and $T = 0$ for simplicity,

$$\rho\omega^2 = (\rho g + j_{0y} B_{0x}) k_r \sqrt{\frac{2}{\alpha}}$$

$$k_i = -k_r,$$

which predicts that a strong magnetic field along the propagation direction shortens the wavelength, and, more importantly, leads to strong damping of surface waves within one wavelength. Note that the values of α are typically larger than unity in the fusion reactor application for parallel propagating waves while $\alpha \ll 1$ in the experiments reported in the next section.

F. Summary of linear theory of MHD surface waves

A short summary on theory of the linear MHD surface waves with horizontal magnetic field and current is in order before describing detailed experimental apparatus and results. In the small magnetic Reynolds number limit or when the induction is negligible and the self-field due to imposed electric current is small, the wave dispersion is given by Eq.(18). Only the component of the Lorentz force with parallel B and perpendicular j contributes to the dispersion (this is due to a cancelling of j_{0x} by j_{1z}, which arises to keep the current confined to the gallium surface). As a result, a magnetic field perpendicular to the propagation direction affects neither the wavelength or damping of surface waves. A parallel magnetic field damps waves in liquid with depth on the order of a wavelength and deeper. In liquid much shallower than one wavelength, vertical fluid motion is suppressed and the waves no longer bend field lines, leading to no damping. For the damped waves, the damping efficiency depends on the dimensionless parameter, $\alpha = B_{0x}^2/\rho\eta\omega$, and the waves are weakly damped when $\alpha \ll 1$ and strongly damped when $\alpha \gg 1$.

Next, experimental studies of MHD surface waves in a table-top device are described in detail. The experiments do not cover the full parameter regimes in which the theory is valid. More specifically, the experiments are limited to the cases when no current is imposed and $\alpha \ll 1$ in the deep liquid limit. The small magnetic Reynolds condition is always satisfied.

III. EXPERIMENTAL APPARATUS

We have constructed an experiment to study the properties of liquid gallium surface waves in an applied magnetic field. Figure 2 illustrates the major components of the experimental apparatus: the gallium tank, wave driver and paddle, magnetic field coils, and surface diagnostics. A non-invasive diagnostic measures the the waves by reflecting multiple laser beams off the surface and onto a screen, which is filmed by a camera. A PC-based Labview program with a National Instruments PCI-1671E board controls the experiment by controlling the magnetic field strength, gathering data, gating the wave driver, and digitizing the images from the camera. Below we briefly describe each component of the above experimental apparatus; a more detailed discussion of the experimental setup, including photographs, can be found in one of the author's Bachelor thesis.[17]

A. Gallium tank

Gallium, which melts at about 30 C, is an ideal metal for table-top liquid metal studies. It has a low melting point, is believed to be non-toxic, and the oxidation is confined to a skin layer. Other candidate metals suffer some serious drawbacks. Mercury, which was used by brave experimentalists of the 1950s and 1960s[18,19], is highly toxic and has a high vapor pressure; today it would require prohibitive safety measures. Liquid lithium has potential applications to fusion reactors, and thus begs its own research[2]. However, liquid lithium is
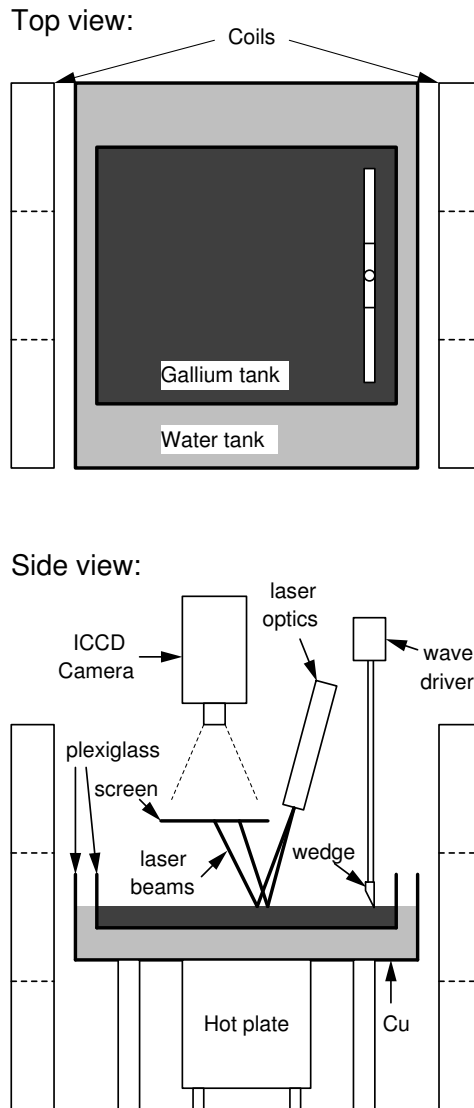
FIG. 2: Experimental setup for study of MHD surface waves in liquid gallium: top view (top panel) and side view (bottom panel).

not an easy-to-handle metal for a table-top experiment because it is reactive with water and air. Liquid sodium, another alkali metal, has similar properties as lithium and is yet more reactive[20].

Approximately 1400 cc of gallium is held in a square plexiglass tank which has a side length of 37.8 cm and a height of 5 cm. The depth of the gallium layer is about 0.9 cm, which satisfies the condition for the deep liquid limit for the most cases in our experiments except the lowest frequencies. The size of the tank is constrained by the cost of gallium, but must be large enough to minimize boundary effects. The gallium tank sits in a larger water tank, which serves as a heat reservoir.

One might suppose that to minimize the effect of side boundaries, the tank must simply be wider than both gallium's capillary length (about 0.35 cm), and the characteristic length of viscous boundary layers. However, the capillary boundary effects are more pernicious, and, in fact, the tank must be made as wide as possible. The gallium generally does not wet the plexiglass walls evenly, and ths non-uniform meniscus at the boundaries scatters the single incident k-vector and creates non-planar waves, and interference, downstream. Thus, in contrast to larger water wave experiments (with flumes less than meter wide and tens of meters long), this small gallium experiment is nearly square in aspect ratio.

The end boundary also needs special attention. Since our aim was to observe traveling waves, one possibility is to find some boundary at the far end that simulates an infinite tank, like impedance matching on a transmission line. Reflections from the end boundary (opposite the side from which waves are driven) complicate the patterns on the surface, and the 7-point laser diagnostic we used does not adequately resolve the counter-propagating waves. In the end, it is found that the best way to make a precise measurement of the wave is to use transient data, taken before reflected waves could return to the measurement location.

B. Wave driving hardware

The paddle design is another way in which this experiment deviates from larger hydro-dynamics experiments. While those experiments use large paddles hinged to the bottom or large wedges to drive waves, early tests we conducted in water and gallium found that wedge-type wave drivers caused splashing if the wedge angle is large (45°). For the experi-

12

ments reported here, we used a wedge with a smaller angle of 31° or an edge of 1/16 inch copper sheet. Unlike the wedge-type paddles, which drive waves by moving volumes of fluid, this kind of paddle pulls up and down on the surface with surface tension. Both paddles were about 34 cm wide, about 90% of the width of the tank. To drive planar waves with a single $\mathbf{k}$, it is very important to have uniform contact along the length of the paddle. When setting up experiment runs, it was important to optimize the planarity of the waves, which we checked using the laser diagnostic described below.

The paddle motion is driven in by the wave driver, an electro-mechnical device (Mechanical Vibrator SF-9324 from Pasco Scientific) similar to a speaker, but more robust and magnetically shielded. The input sinuisoid comes from a signal generator, gated by the experiment control, through a power amplifier. Prior to experiments using gallium, the wave driving hardware was tested using water with and without magnetic field. It was found that the driven waves in water were not affected by presence of a magnetic field, confirming that the wave driving hardware is insensitive to the magnetic field.

C.   Magnetic field coils

In our experiment we have used two pairs of "L-2" coils in a magnetic mirror configuration to provide a relatively uniform, DC magnetic field. The coils, of outer diameter 49.8 cm, are separated by 50.8 cm. Currents of up to 500 A create a field of up to $B_0 = 400$ Gauss at the center in between the coils. Because the gallium tank sits in the midplane of the coils, there is no vertical component to the magnetic field at the liquid surface.

D.   Laser surface diagnostic

To measure the surface waves, we reflect lasers off the surface and onto a screen filmed by an Intensified CCD (charge-coupled device) camera (by ITT Corp.). A passing wave distorts the local angle of the gallium surface and perturbs the laser spot on the screen from its flat-surface position. When the wave amplitude a is small, the deflection of the laser spot is proportional to the slope of the passing wave; the diagnostic thus directly measures the wave steepness ka, where k is the wavenumber. Measuring the relative phases of multiple points on the surface determines the wave number k, and whence a.

The experiment, once configured, is triggered off of a camera gating pulse. Thus, the camera frames correspond to exactly the same points in time in each experiment, confirming that the experiments are highly repeatable. A similar technique was implemented in a recent experiment on (non-MHD) surface wave in mercury[21].

The diagnostic consists of a laser rail, on which the laser (2 mW, He-Ne by Uniphase Model 1101P), and associated optics are mounted, a screen near the gallium surface, and an ICCD camera. Following optics to focus the laser spot on the surface, a diffracting beam splitter (a dot-matrix projection head from Edmunds Optics) splits the laser beam into a diverging matrix of beams, and a mask blocks all but the central row of up to 7 beams. The resultant beams lie in a plane, whose intersection with the plane of the gallium surface is a line parallel to the direction of wave propagation.

The camera takes 60 frames per second (de-interlaced), which are digitized by a National Instruments NI-1407 series frame grabber board and saved to disk. The image intensification hardware on the camera allows for controlled gating of the exposure time; typically, gate widths of 100 μs to 1 ms were sufficient to freeze the laser spot in each frame.

We now present a way to map the laser spot measurements back to the wave motion, valid for small-amplitude waves and diagnostic laser beams that come in close to vertical. Figure 3(b) shows a picture of the laser reflection in the x-z plane for waves propagating in the x-direction.

Figure 3(a) shows a schematic picture of a laser reflecting from a flat surface at x_0 and intersecting the screen at the position r_0. When a wave passes, the angle of the surface changes and the laser spot shifts to $r_0 + \Delta r$. We now correlate the motion of the spot on the screen, $\Delta r(t)$, with the motion of the free surface $\delta(x, t) = a \sin(kx - \omega t)$.

The angle of incidence of the laser beam, θ_0, will be a different value for each of the 7 incident laser beams, because the beams diverge from one another. It will however, be treated as small; the largest incident angle was 4 degrees. We discuss below how to precisely calibrate the θ_0's from a few simple, *in situ* measurements. The flat-surface position of the laser spot on the screen is $r_0 = x_0 + d \tan(-\theta_0)$, where d is the distance of the screen from the gallium surface.

In general, a passing wave not only changes the angle that the ray reflects off at, but also changes the position where the ray intersects the surface, and thus the surface point that the laser samples. However, this effect can be neglected in the first order, as discussed
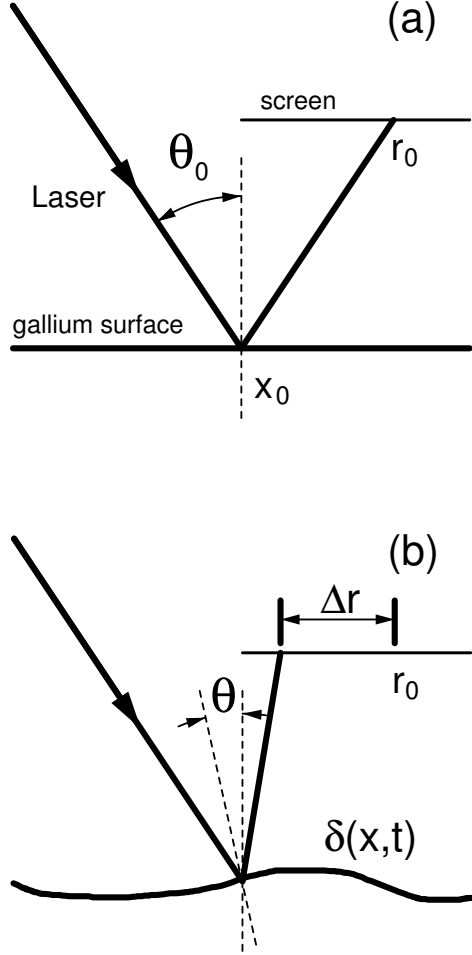
FIG. 3: Laser reflection from the fluid surface: (a) flat surface; (b) surface with waves.

below. In this first approximation of small θ_0 and wave amplitude, the laser always reflects off the surface at the point $(x, z) = (x_0, 0)$. The surface normal at this point due to traveling waves is $\mathbf{n}(t) = \nabla(z - \delta(x, t)) = [ka \cos(kx_0 - \omega t), 0, 1]$. (The laser rays also have a finite component in the y-direction. However, the projection of the incident and reflected rays onto the $x - z$-plane does not depend on it.) Let θ be the inclination of the surface normal. $\tan \theta(t) = ka \cos(kx_0 - \omega t)$

With this definition of θ and θ_0, simple geometry shows that the angle of reflection is $2\theta - \theta_0$. Thus, the motion of the spot on the screen will be

$$
\begin{aligned}
\Delta r(t) &\approx d \tan(2\theta - \theta_0) - d \tan(-\theta_0) \\
&\approx 2dka \cos(kx_0 - \omega t),
\end{aligned} \tag{23}
$$

if $\theta \sim ka \ll 1$ and $\theta_0 \ll 1$. The factor kx_0 affects the phase of the laser motion on the screen.

15

Since the reflection positions $\{x_0\}$ can be precisely calibrated, it is possible to experimentally measure k by comparing the phases of the 7 laser spots.

We now discuss the lowest order corrections to these formulae. First, in the expression above we have used small-angle approximations for the tangent; thus corrections to the above formula will be proportional only to second-order products of ka and θ_0. We also introduce errors by assuming that the reflection always occured at $(x_0, 0)$. The next approximation of the reflection point is $[x_0 - \delta(x_0, t)\theta_0, \delta(x_0, t)]$. The small shift of the reflection position has two effects: first, there will be a correction to the surface normal, and second, the laser will reflect from a different surface height. The former can be evaluated from a Taylor expansion of the surface normal about x_0:

$$n_x \approx n_{x_0} + \left.\frac{\partial n_{x_0}}{\partial x}\right|_{x_0} (x - x_0)$$

The correction to the above formula (23) is therefore of order $ka\theta_0$, since taking the derivative of δ is proportional to k and the position shift is of order $a\theta_0$. This correction, then enters at the same order as the corrections to tangent. Next, the second finite amplitude effect changes the total distance the laser travels, shifting the position of the spot on the screen by about $2\delta(t)\tan\theta_0 \approx 2a\theta_0$. Comparing this to our linear formula (23), we can see the correction is of order a/d, which is small in our setup: $a \sim 0.1$ mm while $d \sim 10$ cm.

E.   Calibrations

To calibrate the laser diagnostic, first the beam splitter was carefully characterized to determine the inter-beam divergence. Once this is known, a few still frames taken with the laser in place in the experiment is sufficient to calibrate the angle θ_0 of each ray and the height of the screen, to better than 1%. The first still frame is taken with the screen moved intersect the beams on the way to the gallium. The second is taken with the screen in its normal position, so that the laser beams intersect the screen after reflecting off the flat gallium surface. The difference in laser spots between the two frames is only due to the path of the lasers between the plane of the screen and the plane of the gallium surface. From knowledge of the inter-beam divergence and these measurements, one can determine the height of the screen, the angle θ_0 of each laser, and the location on the surface that each laser measures. Finally, a still frame taken of a grid of points in place of the screen maps

pixels to real-world units and in principle allows for correction of any optical distortion in the camera optics. (We did not, however, observe any distortions in our optical setup.)

F. Procedures for data analysis

The camera takes images of the laser spot motion, which are digitized and saved. For analysis, an IDL (Interactive Data Language) program was written to find the laser spots in each frame, by finding the regions with the brightest points. The location of the spot is determined consistently by a mass-weighted average of the light intensity over a small region containing the spot, after removing background light. The error in the location of the spot center is assigned to be 1 pixel (since the centroid is determined more accurately than this). As mentioned before, because we can control the camera shutter gating, we can gate for a short enough time so that the laser spots do not smear in the frames.

After finding the lasers in each frame, a time series of spot motion is assembled at each surface location. It is found that a sinusoid is an excellent fit to each time series, consistent with the Eq.(23). From the fitting parameters, we can find the frequency, relative phase of the spots, and the amplitude of the spots motion, from which we find ka at each surface location.

IV. EXPERIMENTAL RESULTS

Descriptions of experimental results are divided into two sections: wave propagation and wave damping, which correspond to the real and imaginary parts of the dispersion relation, respectively, as exemplified by Eqs.(20) and (21) in the deep liquid and weak magnetic field limits. Discussions are included in each section following the descriptions of results.

A. Wave propagation without magnetic field

Figure 4 shows an example of the measured movements of 7 reflected laser spots on the screen as functions of time. We focus on waves in the early times after the initiation before they are reflected from the end boundary to minimize the effects due to standing waves (see
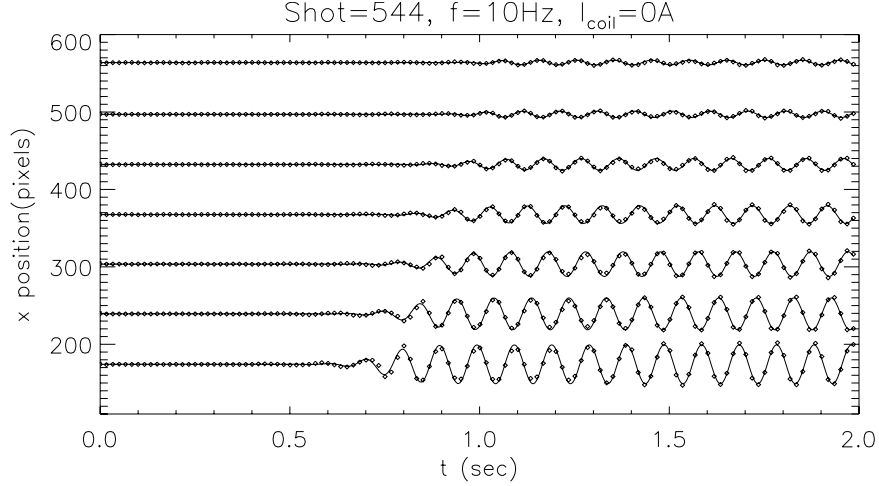
17

FIG. 4: Examples of measured movements of reflected laser spots on the screen as functions of time (diamonds). Solid lines indicate fitted curves to the measurements (see text).

Sec. III.B). The movement of each reflected laser is fitted to the function of

$$\Delta r(t) = \frac{1}{2} \left(\tanh \frac{t - t_0}{\tau} + 1 \right) \Delta r_0 \sin(\omega t - p) + c, \tag{24}$$

where all parameters except t are fitting parameters. Here t_0 represents the arriving time of the waves at each laser and Δr_0 is related to the wave amplitude by Eq.(23),

$$\Delta r_0 = 2dka. \tag{25}$$

The fitting is performed by a nonlinear fitting procedure provided by the IDL package, and the fitted curves are shown by solid lines in Fig.4. The wave frequency $f = \omega/2\pi$ is accurately determined the fitting and is 10.13 ± 0.03 Hz for the example given by Fig.4. The wave phase p is fitted linearly with position x as shown as the solid line in Fig.5(top), and the slope of the line determines the wavenumber, k, or equivalently the wavelength, λ, which is 2.20 ± 0.01 cm for the example given by Fig.4. Consequently, the wave amplitude at each laser is determined by Eq.(25) since all other quantities $(\Delta r_0, d, k)$ are known. The obtained amplitudes are shown in Fig.5(bottom).

In order to measure the dispersion relation of the MHD surface waves, the driving frequency is varied from about 4 Hz to about 12 Hz. The lower frequency is limited by the size of the gallium tank which can only accommodate few wavelengths at lower frequencies. The upper frequency is limited by the time resolution of frame acquisition rate of 60 Hz. While there is no Nyquist frequency *per se*, because the waves are monochromatic and the
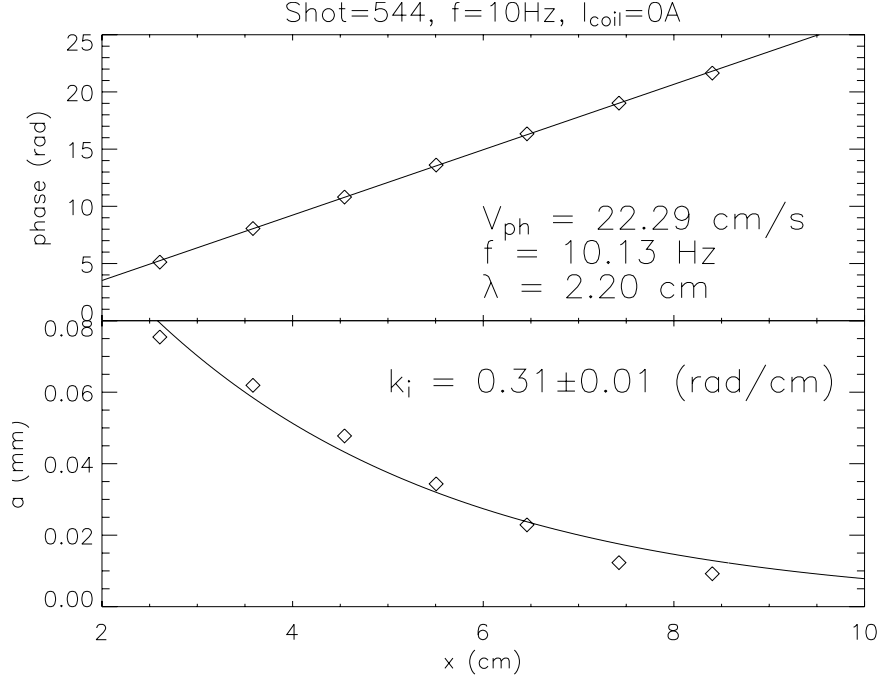
FIG. 5: The wave phase (top) and amplitude (bottom) as functions of x for the example given by Fig.4. The uncertainty of each point is smaller than the symbol size.

wave frequency is approximately known, the fitting routine used still requires good time resolution to converge.

The measured dispersion relation with no imposed magnetic field is shown in Fig.6 as diamonds, which is compared with theoretical predictions by Eq.(18) with $j_{0y} = B_{0x} = 0$,

$$\rho\omega^2 = (\rho g + k^2 T)k\tanh(kh), \tag{26}$$

using the published value of surface tension coefficient[22] (solid line). Agreement is found between experiment and theory only for the low frequencies, but not for high frequencies. The measured wavelengths are shorter than predicted values for a given driving frequency. However, an *ad hoc* surface tension coefficient, lowered by a factor of 2.5, agrees fairly well with the experiment at all frequencies.

The apparent reduction of surface tension is likely due to a thin oxide layer formed on the gallium surface. The oxide layer becomes visible when a clean liquid gallium is exposed to air for a few hours if left still, or appears in only a few minutes if surface waves are driven. A decrease in surface tension due to oxidation is qualitatively consistent with a small chemistry experiment performed by the authors. After covering of small blob of gallium with a coating
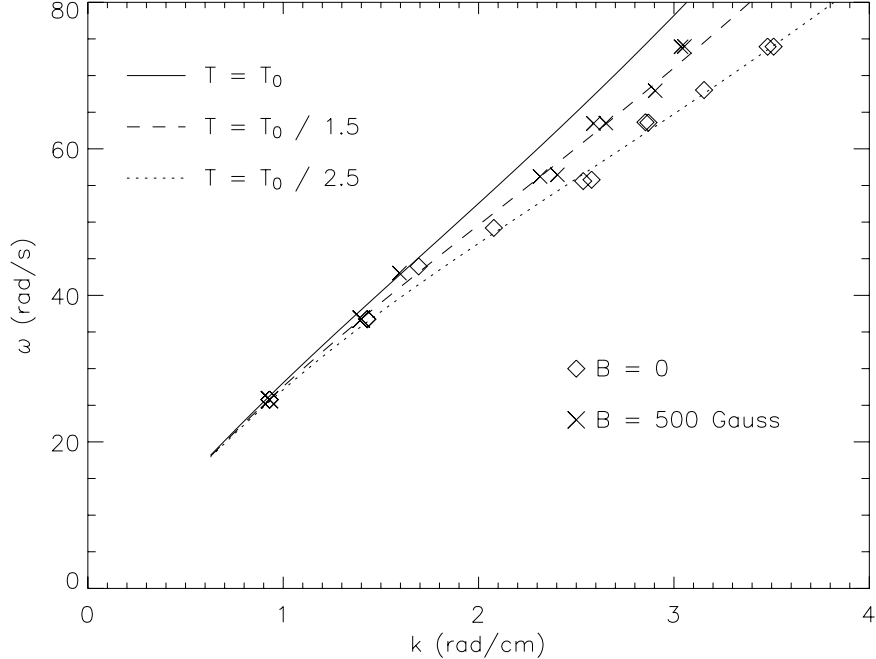
19

FIG. 6: The measured dispersion relation of MHD surface waves in gallium without magnetic field (diamonds) and with B_0=380 Gauss (cross). Theoretical curves by Eq. (26) are shown for three cases: $T = T_0 = 0.718$N/m (solid line); $T = T_0/1.5$ (dashed line); and $T = T_0/2.5$ (dotted line).

of 1 mole hydrochloric acid solution, the surface became very shiny as the acid i cleaned the oxide layer from the surface. At the same time the surface was cleaned, the gallium pulled itself up into a tight ball, implying increased surface tension. Later, as the acid evaporated and the surface re-oxidized, the gallium lost its uniform tight shape, implying that the surface tension decreased.

B.   Wave propagation with magnetic field

The effects of a horizontal magnetic field on the surface wave dispersion relation are studied by repeating the above experiments with varying strength of the applied field. Also shown in Fig.6 are the results obtained under a parallel imposed field of $B = 500$ Gauss at the measurement locations. At a given driving frequency, the wavelength is observed to increase with B. At $B = 500$ Gauss, the lengthened wavelength is still shorter than the predictions using $T = T_0$, but the observed changes are more than 10% at $f \approx 12$ Hz. Interestingly, the measurements agree well with the predictions using $T = T_0/1.5$. To
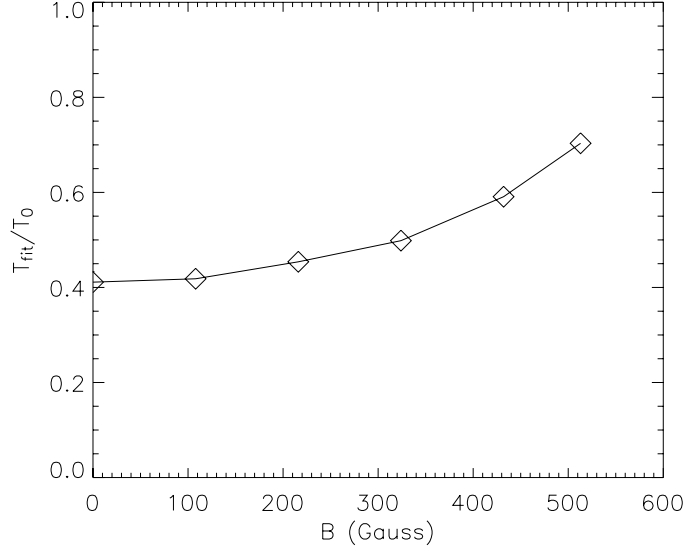
20

FIG. 7: The fitted surface tension coefficient normalized by published value[22] for clean gallium $T_0 = 0.718$ N/m as a function of imposed magnetic field.

quantify the observed changes better, the measured dispersion relation is fitted by Eq.(26) with T as a free parameter. The fitted T is shown as a function of B_x in Fig.7.

The observed change in the dispersion relation of the surface wave propagation due to magnetic field cannot be simply explained by linear theory. According to Eq.(18), the real part of the dispersion relation does not depend on magnetic field if the DC current density is zero. This is better seen in Eq.(26), which is valid in the limit of weak magnetic field ($\alpha = B_{0x}^2/\rho\eta\omega \ll 1$), a condition well satisfied in our experiments. For example, for $f \approx 12$ Hz and $B = 500$ Gauss, $\alpha = 0.022$. The next order corrections to the dispersion is on the order of $\alpha^2 \approx 5 \times 10^{-4}$, which is much smaller than the measured changes. Furthermore, the observed changes cannot be explained by nonlinear effects, which is on the order of the ratio of $\rho(\boldsymbol{V}_1 \cdot \boldsymbol{\nabla})\boldsymbol{V}_1$ to $\rho\partial\boldsymbol{V}_1/\partial t$ (see Sec. II.A) or simply $ka \sim 10^{-2}$. The effect due to omission of the wave-induced magnetic field $\boldsymbol{B}_1$ is also small:

$$\frac{B_1}{B_0} \sim \frac{\mu_0 j_1}{k B_0} \sim \frac{\mu_0 V_1}{k\eta} \sim \frac{\mu_0 \omega a}{k\eta} \sim 6 \times 10^{-5}.$$

We therefore seek explanations outside of the physics in the linear MHD dispersion relation. One possible explanation of the observed changes in effective surface tension force with an imposed magnetic field is changes in atomic physics in the surface oxide layer or the adjacent pure gallium layers . The structure of surface of liquid metal has been a hot topic in recent years, especially after rapid development of experimental techniques, such as x-ray

21

reflectivity measurements, to directly study the surface structure. A recent review paper is given by Penfold on this topic[23]. A theoretically predicted phenomenon called surface-induced atomic layering[24] due to the sharp discontinuity in density across a liquid-vapor surface has been confirmed experimentally[25]. The effect of oxidation on gallium surface has also been studied[26]. It was found that the oxide layer has a uniform thickness of about 5 Å, which does not increase with further oxygen exposure and temperature increase, suggesting that the oxide layer provides rigidity to the surface and thus may cause wave damping (see later). The dependence of these surface properties on the magnetic field has been reported neither experimentally nor theoretically. However, it would not be surprising to have some dependences on magnetic field since liquid gallium has larger degrees of covalency (less close to a free-electron metal) and directional bonding[23]. We should note that the dispersion relation remains unchanges when the magnetic field is imposed horizontal but perpendicular to wave propagation[17]. This fact constrains of theory of surface tension modification by a magnetic field: the magnetic field can only modify the surface tension along the direction of the magnetic field.

C. Wave damping without magnetic field

The linear theory predicts that waves interact with a parallel magnetic field, leading to damping in deep fluids [Eq.(21)]. However, as shown in Fig.5, wave damping exists even without magnetic field. To quantify the wave damping rate, the amplitudes are fitted to the function of

$$a(x) = a_0 \exp[-k_i(x - x_0)], \tag{27}$$

where a_0 and k_i are fitting parameters and x_0 is the x position of the first laser measurement. The magnitude of k_i characterizes the damping rate. The fitted curve is also shown in Fig.5, where the error in k_i, δk_i, is estimated by equating the measurement uncertainties $\delta a(x)$ to $-a_0(x - x_0) \exp[-k_i(x - x_0)]\delta k_i$. (One should note that there exist also systematic errors in k_i due to deviations from the perfect e-folding beyond statistical uncertainties in the measurements. Using residual fitting errors, the systematic errors in k_i are estimated to be about 4 times larger than the statistical counterparts.) Figure 8 shows that the normalized damping rate, k_i/k, increases with k, but saturates at about 0.1 at large k.

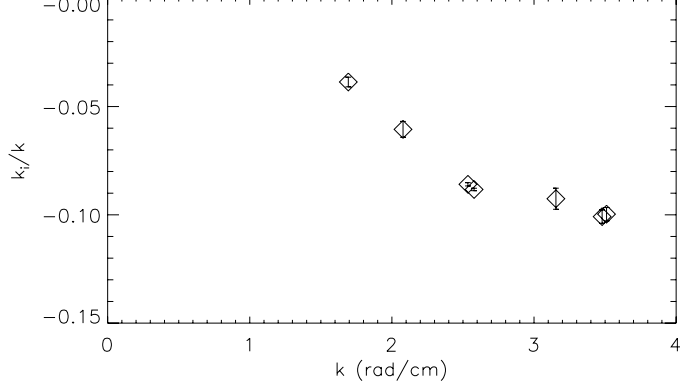Absent a magnetic field, waves can be damped by finite viscosity, which has been ignored

FIG. 8: The normalized wave damping rate, k_i/k, versus k without magnetic field.

in the linear theory described earlier because of its smallness. Here we estimate the viscous damping rate as following. Let v be characteristic fluid velocity due to the wave motion, then the dominant viscous force is given in deep fluids by

$$F_\nu = \rho\nu\frac{\partial^2 v}{\partial x^2} \sim \rho\nu k^2 v,$$

where ν is kinematic viscosity. Therefore, the wave energy decays as

$$\frac{\partial}{\partial t}\left(\frac{1}{2}\rho v^2\right) = -F_\nu v = -\rho\nu k^2 v^2,$$

which leads to

$$a(t) = a_0 \exp(-\nu k^2 t) \qquad (28)$$

since $v = \partial a/\partial t = \omega a$. We note that Eq.(28) is consistent with more rigorous derivations[17,27] within a factor of 2. Setting $t = x/v_{\mathrm{ph}} = kx/\omega$ in Eq.(28) leads to $a(x) = a_0\exp(-k_i x)$, where

$$\frac{k_i}{k} = \frac{\nu k^2}{\omega} \simeq (1-4) \times 10^{-4}, \qquad (29)$$

using the published value[22] for gallium viscosity $\nu \simeq 3\times 10^{-7}\mathrm{m^2/s}$ and the measured values for other quantities. There is also a viscous drag effect due to the friction between the oscillating fluid and stationary tank boundaries[27]. Landau and Lifshitz calculate the temporal damping rate to be

$$\gamma = \frac{1}{2\sqrt{2}}\frac{2h+w}{wh}\sqrt{\nu\omega}, \qquad (30)$$

which depends the fluid depth h, and the tank width w. As might be expected, since the damping gives the energy dissipated per unit energy in the fluid, and all the energy dissipation occurs at the boundary, the expression incorporates the ratio of the area of
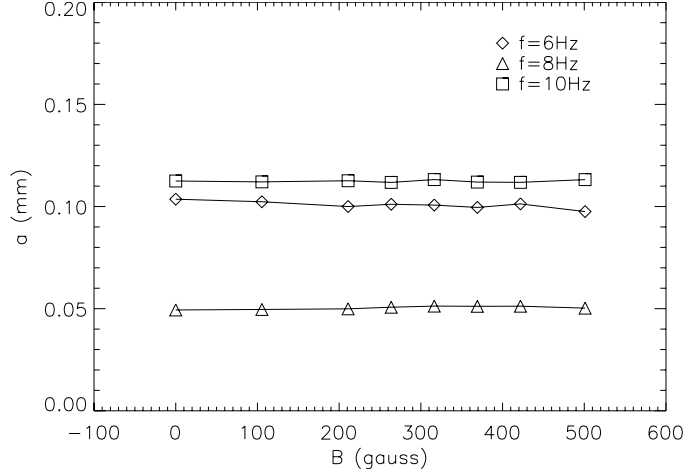
23

FIG. 9: The wave amplitude measured by the first laser as a function of magnetic field perpendicular to the propagation direction for several frequencies.

contact with the wall ($2h + w$ per unit length) to the fluid volume (wh per unit length). Using the tank width of 40 cm, and depth of 1 cm, one can estimate that the convective damping rate due to this effect is $k_i/k \sim 2 \times 10^{-3}$. Therefore, the viscous drag at the boundary is more important than the internal viscosity, but it, too, is too small to explain the observed wave damping without magnetic field.

An alternate explanation again can be based on existence of the surface oxide layer, which has been described in Sec. III.A and III.B. Wave motions bend the oxide layer, which is likely semirigid and thus consumes wave energy. Qualitatively, it was observed that the gallium surface becomes less excitable as the oxide layer forms. In fact, deviations from the exact exponential decay, as seen in Fig.5, may be due to non-uniformness of the oxide layer, which often is visible. We note that in general the wave damping due to this mechanism can also depend on the wave amplitude, and this effect was not investigated in our experiment (Fig.8). On the other hand, quantitative theoretical estimates are not possible without detailed knowledge of physical properties of the layer, which is beyond the scope of the present paper.

D. Wave damping with magnetic field

According to the linear theory described in Sec.II, MHD surface waves in the deep liquid limit are not damped by a perpendicular magnetic field to the propagation direction, but not
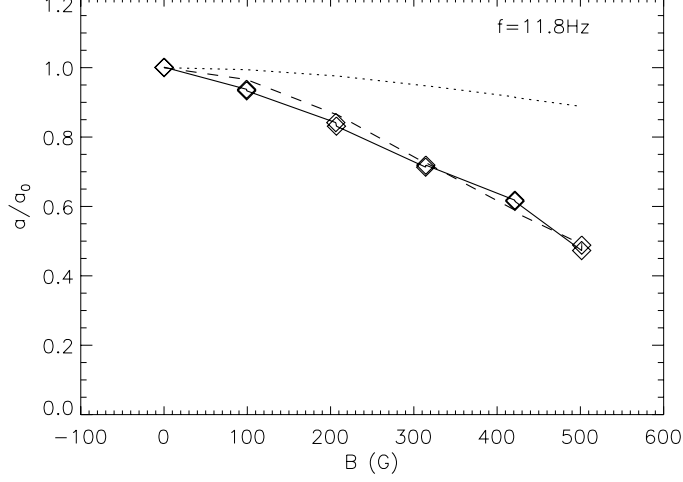
24

FIG. 10: The wave amplitude measured by the first laser as a function of magnetic field parallel to the propagation direction. The dotted and dashed lines represent predictions by linear theory using actual distance between the paddle and measurement (Δx) and a distance of $6\Delta x$, respectively.

by a perpendicular magnetic field. These predictions are basically confirmed by experiments. Figure 9 shows the wave amplitudes as a function of magnetic field perpendicular to the propagation direction for several frequencies while everything else is kept the same. No wave damping by magnetic field is observed. In contrast, the waves are damped by an imposed magnetic field along the propagation direction, as shown in the single point measurements. Fig. 10. The plotted amplitudes are normalized by the amplitude without magnetic field. It is seen that the wave amplitude is reduced by a factor of 2 when a magnetic field of 500 G is imposed.

Linear theory predicts wave damping by a parallel magnetic field as shown in Eq.(21). The damping rate, given by

$$\exp\left[-\frac{B_{0x}^2 \omega k_r}{2\eta(\rho\omega^2 + 2Tk_r^3)}\Delta x\right],\tag{31}$$

where $\Delta x \simeq 4.1$cm is the distance between the paddle and the measurement location, is also shown in Fig.10 as the dotted line. The observed damping rates are much larger than the predictions, but would be consistent with predictions if instead $6\Delta x$ was used in Eq.(31) as also shown in Fig.10 as the dashed line. Here we need to point out that the wave damping given by Eq.(31) accounts only for the MHD effects during the wave *propagation*, but not for the wave *generation* by the paddle, which is also subject to the MHD interactions. Such MHD effects are well conceivable since the cross-field motions tend to bend the magnetic
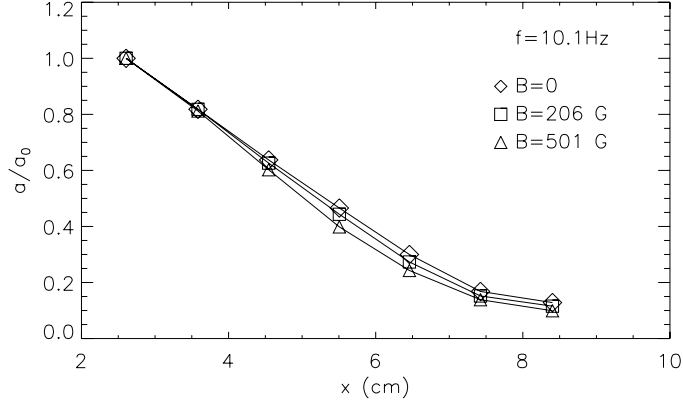
25

FIG. 11: The normalized wave amplitudes as functions of x for several magnitudes of magnetic field parallel to the propagation direction.

field lines in a probably nonlinear fashion, although detailed theoretical modeling is beyond the reach of the present linear theory. The observed damping enhancement likely reflects such MHD effects during the wave generation. Note that experiments in water did confirm that the wave driving hardware alone is unaffected by the magnetic field[17]

Furthermore, the wave damping due to magnetic field parallel to the propagation direction is observed in between the measurements at 7 locations. As an example, Fig.11 shows the normalized wave amplitudes as functions of x for $B = 0$, 206 G, and 501 G, respectively. It is clearly seen that the wave is damped more rapidly when a stronger magnetic field is applied. To better quantify the wave damping, measurements at each given magnetic field are fitted to the function shown in Eq.(27) to obtain a spatial damping rate k_i. The results are shown in Fig. 12 as squares. Despite certain scatters in the obtained damping rates, a trend for increased damping rate with magnetic field is apparent. Note that the scatter in the data points is on the same order of the error exemplified in Fig. 5. The theoretically predicted damping rates given by Eq.(21), $k_i(B)$, are calculated by using the measured values for all other parameters. Plotted also in Fig.12 as the dashed line is $k_i(0) + k_i(B)$ where $k_i(0)$ is the measured damping rate at $B = 0$. The agreement is reasonable given the scatter and errors in the experimentally determined damping rates.
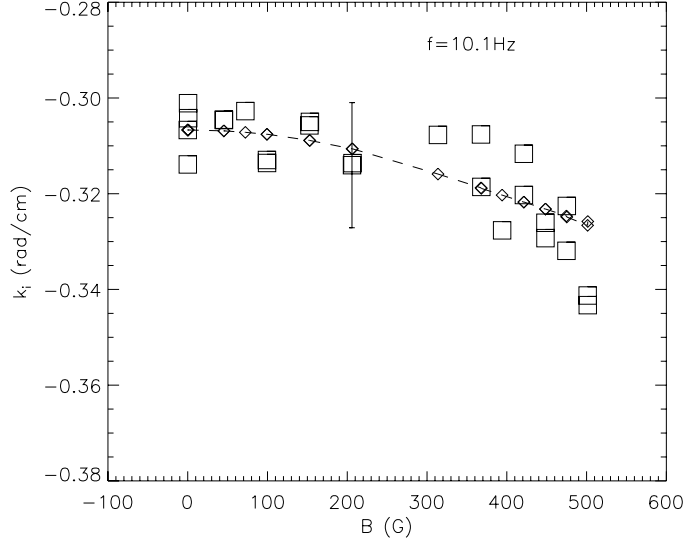
26

FIG. 12: The wave damping rate (squares) as a function of magnetic field parallel to the propagation direction. The dashed line represents predictions by linear theory (see text).

V. IMPLICATIONS TO FUSION APPLICATION

Given theoretical and experimental results and their physics understanding described in the previous sections, discussions are in order with regard to their implications to the proposed application of a free-surface liquid metal first wall in the fusion reactors[2–4]. Below we discuss two specific effects: magnetic damping of surface waves, and an instability when the Lorentz force is used to support a free-surface liquid metal layer against gravity.

A. Magnetic damping of surface waves

An important dimensionless parameter here is $\alpha = B^2/\rho\eta\omega$. For a typical magnetic field strength of 10 T in the magnetic fusion reactors, α is much larger than unity unless $f > 100\text{kHz}$ for lithium or $f > 10\text{kHz}$ for gallium. However, the surface tension becomes important and strongly stabilizing [Eq.(21)] at these high frequencies. Therefore, one expects that the large magnetic fields in the magnetic fusion reactors will stabilize surface disturbances very effectively along the field direction in the deep fluid limit. In addition, a finite vertical magnetic component will further stabilize the surface as shown in previous studies[14,18,28].

However, there is no magnetic damping on disturbances propagating in a horizontal,

27

but perpendicular, direction, as shown in the previous sections. Even for the case when the disturbances propagate parallel to magnetic field, the damping effect does not exist if the wavelength is much longer than $2\pi h$ so that the liquid is shallow, *i.e.*, $kh \ll 1$. (We note that this is a theoretical result since our experiment did not cover this regime.) If $h = 5$mm, then the critical wavelength above which there is no large stabilizing effect from magnetic field is about 3cm. Therefore, in the application of a free-surface liquid metal first wall in a fusion reactor, it may not be possible to depend on magnetic damping to suppress disturbances. However, surface conditions, such as existence of an oxide layer, may provide more effective stabilization for possible disturbances, as observed experimentally in the previous section. Of course, the detailed atomic physics and chemistry, as well as their manifestation as surface tension, need to be understood before they can be better applied in the reactor environment.

B. Stability of a liquid metal layer supported by Lorentz force against gravity

In order to completely cover the plasma in a fusion reactor, some parts of a liquid metal layer need be supported against gravity. One proposed method is to use the Lorentz force by inducing electric current in the liquid metal with an appropriate angle to the background magnetic field so that the resulting Lorentz force is upward to offset the gravity force[4]. This scheme works if the supported liquid metal is stable. However, the obtained dispersion relation, Eq.(18), suggests that this is not the case.

Using the coordinate shown in Fig.1, now the gravity force ρg points upward and the Lorentz force, $|\boldsymbol{j}_0 \times \boldsymbol{B}_0| = |j_{0x}B_{0y} - j_{0y}B_{0x}| \geq \rho g$, points downward. Thus the term ρg in Eq.(18) needs to be replaced by $-\rho g$. As discussed in Sec. II.D, only one of the two terms of the Lorentz force, $j_{0y}B_{0x}$, appears in the dispersion relation. This only term will also disappear when the x direction or the propagation direction is set to be perpendicular to $\boldsymbol{B}_0$. The resultant dispersion relation then becomes

$$\rho\omega^2 = (-\rho g + k^2 T)k\tanh(kh),\tag{32}$$

which predicts instability for sufficiently small k or long wavelength. This is essentially the Rayleigh-Taylor instability. Figure 13 shows the growth rates for both lithium and gallium cases. The critical wavelength is determined by the surface tension, which may
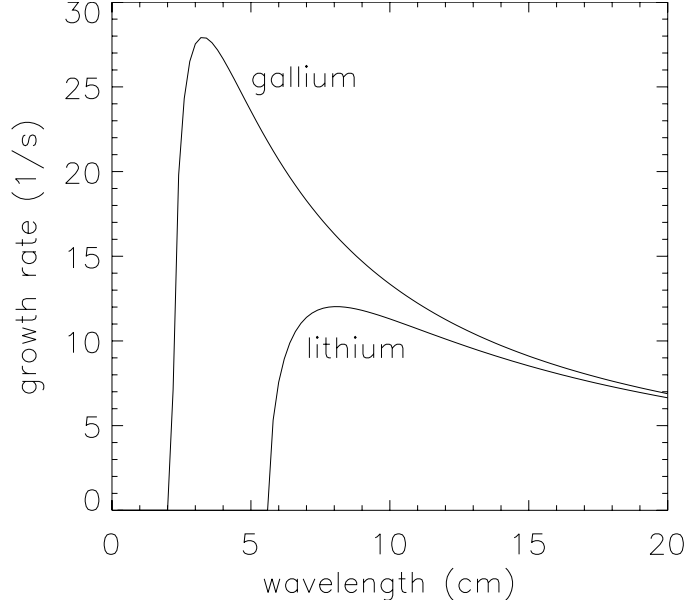
FIG. 13: The growth rate as functions of wavelength for lithium or gallium layer supported by the Lorentz force against gravity in the deep liquid limit.

vary depending on the surface conditions, as described in this paper. The typical growth time is on the order of 0.1 s for lithium, which sets the maximum time scale for the liquid metal to stay in the layer supported by the Lorentz force. This can be translated into a minimum speed with which liquid metal is forced to flow across certain distances in the reactor chamber. For example, for a distance of 1 m, the minimum speed is 10 m/s if only one e-folding time is allowed for this instability to grow. Again, the existence of a surface oxide layer can slow down its growth.

VI.   CONCLUSIONS

Effects of magnetic field on surface waves on liquid gallium are studied in detail both theoretically and experimentally in the small magnetic Reynolds number limit. Theoretically, a linear dispersion relation is derived when horizontal magnetic field and electric current is imposed, including effects from surface tension. No wave damping is found in the shallow liquid limit ($kh \ll 1$) while waves will damp in the deep liquid limit ($kh \gg 1$) if travelling parallel to the magnetic field. Under a weak magnetic field ($B^2/\rho\eta\omega \ll 1$), waves are weakly damped with no effects on propagation characteristics while in the opposite limit the waves are strongly damped with shortened wavelengths. Experimentally, the planar MHD surface

29

waves on liquid gallium are studied in detail with a weak magnetic field and in the deep liquid limit by using a computer-controlled paddle in a table-top device. A non-invasive diagnostic accurately measures surface waves at multiple locations by reflecting an array of lasers off the surface onto a screen, which is recorded by an Intensified-CCD camera. The measured dispersion relation is consistent with the linear theory with a reduced surface tension likely due to surface oxidation. It is observed that surface waves are damped when a horizontal magnetic field is imposed parallel to the propagation direction. No damping is observed with a perpendicular magnetic field. These results are in excellent agreements with the linear theory. The existence of a strong wave damping without magnetic field suggests the importance of the surface oxide layer. Implications to the liquid metal wall concept in fusion reactors are discussed. Magnetic damping can suppress surface disturbances with short wavelengths propagating along the magnetic field, but waves with long wavelengths or propagating across magnetic field are unaffected. A liquid metal layer supported by the Lorentz force against gravity is unstable to the Rayleigh-Taylor instability when a perturbing wave vector is perpendicular to the magnetic field and its wavelength is sufficiently long, possibly leading to a practical limitation of these applications.

Acknowledgements

---

[*] Electronic address: `hji@pppl.gov`

[†] Current address:Physics Department, Massachusetts Institute of Technology, Cambridge, Massachusetts

[‡] Current address:Department of Physics and Astronomy, University of California, Los Angeles, California

[1] E. Northrup, Phys. Rev. **24**, 474 (1907).

[2] S. Molokov and C. Reed, Technical report, ANL/TD/TM99-08, Argonne National Laboratory (unpublished).

[3] N. Morley *et al.*, Fusion Eng. Design **51-52**, 701 (2000).

[4] M. Abdou *et al.*, Fusion Eng. Design **54**, 181 (2001).

[5] L. Zakharov, Phys. Rev. Lett. **90**, 045001 (2003).

[6] H. Rappaport, Phys. Plasmas **8**, 3620 (2001).

[7] G. Murty, Arkiv För Fysik **19**, 499 (1961).

[8] S. Breus, Tech. Phys. **5**, 960 (1961).

[9] G. Murty, Arkiv För Fysik **19**, 483 (1961).

[10] J. Shercliff, J. Fluid Mech. **38**, 353 (1969).

[11] R. Baker, Nature **207**, 65 (1965).

[12] M. Duc, C.R. Acad. Sc. Paris. Serie A **266**, 738 (1968).

[13] J. C. Rook, Ph.D. thesis, Massachusetts Institute of Technology, 1964.

[14] A. Shishkov, Magnetohydrodynamics **29**, 368 (1993).

[15] V. Korovin, Tech. Phys. **41**, 752 (1996).

[16] M. Schaffer, J. Fluid Mech. **33**, 337 (1968).

[17] W. Fox, Magnetohydrodynamic Surface Waves in Liquid Metal, Bachelor Thesis, Princeton University, 2001.

[18] B. Lehnert, Arkiv für Fysik **5**, 69 (1952).

[19] T. Cowling, *Magnetohydrodynamics* (Interscience Publishers, Inc., New York, 1957).

[20] D. Lide, *CRC Handbook of Chemistry and Physics* (CRC Press, Boca Raton, 2002).

[21] E. Falcon, C. Laroche, and S. Fauve, Phys. Rev. Lett. **89**, 204501 (2002).

[22] T. Iida and R. Guthrie, *The Physical Properties of Liquid Metals* (Clarendon Press, Oxford, 1988).

[23] J. Penfold, Rep. Prog. Phys. **64**, 777 (2001).

[24] J. Allen and S. Rice, J. Chem. Phys. **67**, 5105 (1977).

[25] M. Regan *et al.*, Phys. Rev. Lett. **78**, 5225 (1995).

[26] M. Regan *et al.*, Phys. Rev. B **55**, 10786 (1997).

[27] L. Landau and E. Lifshitz, *Fluid Mechanics* (Butterworth Heineman, Oxford, 1987).

[28] L. Fraenkel, J. Fluid Mech. **7**, 6 (1959).

External Distribution

Plasma Research Laboratory, Australian National University, Australia

Professor I.R. Jones, Flinders University, Australia

Professor João Canalle, Instituto de Fisica DEQ/IF - UERJ, Brazil

Mr. Gerson O. Ludwig, Instituto Nacional de Pesquisas, Brazil

Dr. P.H. Sakanaka, Instituto Fisica, Brazil

The Librarian, Culham Laboratory, England

Mrs. S.A. Hutchinson, JET Library, England

Professor M.N. Bussac, Ecole Polytechnique, France

Librarian, Max-Planck-Institut für Plasmaphysik, Germany

Jolan Moldvai, Reports Library, Hungarian Academy of Sciences, Central Research Institute
    for Physics, Hungary

Dr. P. Kaw, Institute for Plasma Research, India

Ms. P.J. Pathak, Librarian, Institute for Plasma Research, India

Ms. Clelia De Palo, Associazione EURATOM-ENEA, Italy

Dr. G. Grosso, Instituto di Fisica del Plasma, Italy

Librarian, Naka Fusion Research Establishment, JAERI, Japan

Library, Laboratory for Complex Energy Processes, Institute for Advanced Study,
    Kyoto University, Japan

Research Information Center, National Institute for Fusion Science, Japan

Dr. O. Mitarai, Kyushu Tokai University, Japan

Dr. Jiangang Li, Institute of Plasma Physics, Chinese Academy of Sciences,
    People's Republic of China

Professor Yuping Huo, School of Physical Science and Technology, People's Republic of China

Library, Academia Sinica, Institute of Plasma Physics, People's Republic of China

Librarian, Institute of Physics, Chinese Academy of Sciences, People's Republic of China

Dr. S. Mirnov, TRINITI, Troitsk, Russian Federation, Russia

Dr. V.S. Strelkov, Kurchatov Institute, Russian Federation, Russia

Professor Peter Lukac, Katedra Fyziky Plazmy MFF UK, Mlynska dolina F-2,
    Komenskeho Univerzita, SK-842 15 Bratislava, Slovakia

Dr. G.S. Lee, Korea Basic Science Institute, South Korea

Institute for Plasma Research, University of Maryland, USA

Librarian, Fusion Energy Division, Oak Ridge National Laboratory, USA

Librarian, Institute of Fusion Studies, University of Texas, USA

Librarian, Magnetic Fusion Program, Lawrence Livermore National Laboratory, USA

Library, General Atomics, USA

Plasma Physics Group, Fusion Energy Research Program, University of California
    at San Diego, USA

Plasma Physics Library, Columbia University, USA

Alkesh Punjabi, Center for Fusion Research and Training, Hampton University, USA

Dr. W.M. Stacey, Fusion Research Center, Georgia Institute of Technology, USA

Dr. John Willis, U.S. Department of Energy, Office of Fusion Energy Sciences, USA

Mr. Paul H. Wright, Indianapolis, Indiana, USA